UV-absorption and radiation effects in different glasses doped with iron and tin in the ppm range

Doris Ehrt*

Otto-Schott-Institut, Friedrich Schiller University of Jena, Fraunhoferstr. 6, 07743 Jena, Germany

Abstract – Intrinsic and extrinsic ultraviolet absorption and radiation-induced effects were investigated in different glass types, fluorides, phosphates and borosilicates. High-purity glass samples were prepared and their intrinsic absorption was measured in the vacuum ultraviolet region. The influence of doped iron and tin species in the ppm range on the ultraviolet absorption and radiation-induced effects were studied. The maximum of the dominating Fe^{3+} charge transfer band has the lowest energy (4.8 eV) and intensity in the fluoride glass and the highest energy (5.6 eV) and intensity in the borosilicate glass samples. The charge-transfer band for Fe^{2+} has much lower intensity and higher energy (~5.7 eV) than those for Fe^{3+} in all glasses investigated. Photo-oxidation of Fe^{2+} to $(Fe^{2+})^+$ hole centres and glass-matrix-related electron centres by UV irradiation increases the UV absorption drastically in all glasses. The kinetics was measured and simulated depending on the glass matrix. In fluoride and phosphate glasses, Fe^{3+} complexes are very stable against UV irradiation and do not participate in UV-radiation-induced processes. Only in silicate glasses, Fe^{3+} is able to form a $(Fe^{3+})^-$ electron centre defect which decreases the charge transfer absorption of Fe^{3+} near 220 nm, but increase the absorption of hole centre defects, with a maximum at 280 nm. So, the defect generation in the ultraviolet region increases drastically with increasing Fe content in the range 10–200 ppm. Three or four electronic s → p transitions for Sn^{2+} were detected by optical absorption and luminescence spectroscopy shifted to longer wavelength in the range fluoride → phosphate → silicate glass samples. Sn^{4+} absorption bands were found at shorter wavelength in the vacuum ultraviolet region in all cases investigated. Sn^{2+} ions are photo-oxidised under UV radiation very fast, which leads to an decrease of absorption near 200 nm and to an increase near 250 nm. Both Sn^{2+} and Sn^{4+} are involved in the radiation-induced processes. In contrast to phosphate and silicate glasses, tin-doped fluoride glasses are very resistant against UV lamp but not against UV laser irradiation. The mechanisms are very complicated, with maximums and minimums in the defect formation curves. *To cite this article: D. Ehrt, C. R. Chimie 5 (2002) 679–692* © 2002 Académie des sciences / Éditions scientifiques et médicales Elsevier SAS

glass / fluorides / phosphates / iron / tin / UV absorption / UV irradiation

Résumé – L'absorption ultraviolette et les effets induits par l'irradiation, aussi bien de nature intrinsèque qu'extrinsèque, ont été étudiés dans différents types de verres : fluorures, phosphates et borosilicates. Des verres de haute pureté ont été préparés et caractérisés sous vide. Ces verres ont été dopés avec de l'étain et du fer. *Pour citer cet article : D. Ehrt, C. R. Chimie 5 (2002) 679–692* © 2002 Académie des sciences / Éditions scientifiques et médicales Elsevier SAS

verre / fluorures / phosphates / fer / étain / absorption UV / irradiation UV

1. Introduction

The role of glasses as ultraviolet-transmitting materials for special applications has increased in recent years. Fluoride single crystals, mainly CaF_2, and high-purity vitreous silica are well-known materials used for deep UV optics, especially in microlithography [1]. Moreover, for the various applications, a variety of glasses with different properties is required. Fluoro-aluminate and phosphate glasses with high purity are

---

* *Correspondence and reprints.*
  E-mail address: cde@uni-jena.de (D. Ehrt).

also good UV transmitting materials [2–4] with a large intrinsic band gap.

It was found that a traditionally old borosilicate glass type Duran® similar to Borofloat® melted with starting materials of special high purity has also a high transmission in the deep UV range [5–7]. Its structure and properties are mainly determined by the M_2O/B_2O_3 ratio, the so-called boric oxide anomaly [8], so it has almost entirely bridging oxygens, i.e. a very low optical basicity [9] and a large intrinsic band gap for the electronic transitions.

But the real UV transmission is limited by extrinsic charge transfer and $s \rightarrow p$ absorption bands due to trace impurities of metal ions, such as Fe^{3+}/Fe^{2+}, Pb^{2+}, Sn^{2+}, etc., which are influenced by the glass matrix [3, 4, 10–13]. It was shown that both intrinsic and extrinsic absorption are important for UV-radiation-induced defects in the glasses [3–6, 9, 14–20]. The aim of this paper is the investigation of the charge-transfer absorption of Fe^{3+} and Fe^{2+}, the $s \rightarrow p$ absorption of Sn^{2+} and the $d \rightarrow s$ absorption of Sn^{4+} and their role in UV lamp and laser-radiation-induced defects in borosilicate glass samples of special high purity, in comparison with fluoride and phosphate samples. Trace amounts of tin are introduced through the float bath during the Borofloat process [7] or Sn^{2+} dopants are taken as soft reducing agent for Fe^{3+} to increase the UV transmission [6, 16]. Iron is an unavoidable trace impurity in all multi-component glasses produced by melting technique, mainly introduced with the raw materials. Photo-oxidation of Fe^{2+} induced by UV radiation was found in silicate, fluoride and phosphate glasses investigated. On the contrary, Fe^{3+} participates in the radiation processes only in silicate but does not in fluoride and phosphate glasses [4, 14–17, 20].

In previous works, it was shown that small amounts of Sn^{2+} increase the UV defect generation in silicate and borosilicate glasses, but this cannot be generalised for any chosen glass [6, 16, 20]. The mechanisms of formation and healing of radiation-induced defects are very complex, including energy transfer processes.

2. Experimental

For this work, three different glass types, fluoroaluminates, phosphates and borosilicates, with potentially high intrinsic UV transmission were used and melted with raw materials of special high purity (Fe' < 1 ppm, other metals < 0.5 ppm) under oxidising and reducing conditions. The batch compositions and some properties measured on un-doped basic glass samples are given in Table 1. The basic batches were doped with iron and tin components in the ppm range melted under the same oxidising and reducing conditions. Impurity content and redox states were analysed by different methods, chemical, ICP–OES, optical absorption and luminescence analysis. The resulting glass samples had good optical homogeneity. Refractive index values, n_λ, were obtained on a Pulfrich refractometer with an error $\pm 2 \times 10^{-5}$. The dispersion coefficient, $v_e = n_e - 1/n_{F'} - n_{C'}$, was calculated from the measured values n_λ. Sample plates (thickness 0.2–10 mm) were produced for the optical absorption and luminescence measurements and the radiation experiments. The optical absorption spectra in the range of 190–3200 nm were recorded with an error < 1% using a commercial double beam spectrometer and other apparatus for the vacuum UV region (120–200 nm) with an error < 15%. Sample plates were irradiated at room temperature by strong broadband UV lamps (performance density 1500 W m^{-2} in the range 230–280 nm with the XeHg and 190–280 nm with the HOK Hg lamp). For laser-radiation-induced defects, ArF (193 nm), KrF (248 nm) and XeCl (308 nm) excimer lasers (pulse energy 70–500 mJ cm^{-2}, performance density to 10^{11} W m^{-2}, pulse length ~30 ns, repetition rate 1–20 Hz) were used. The absorbance ($E_\lambda = \log T_0/T$, with T_0 the transmission without sample, T the transmission with sample) was recorded with a commercial spectrometer before and after irradiation. The induced absorbance was expressed as an absorption coefficient, $\Delta E/d$ (in cm^{-1}). All spectra were fitted by Gaussian bands, using the commercial PeakFit separation and analysis software [4]. The number of bands was minimised, correlated with different irradiation and annealing experiments, and EPR measurements. EPR measurements were performed on plate samples in comparison with a set of DPPH standards with different spin numbers, using a commercial spectrometer (Bruker ESP 300 E) at room temperature. The annealing of radiation-induced defects was measured at room temperature both with and without lamp or laser radiation, and with thermal treatment below the T_g temperature of the glass samples. The density of the glass was determined using Archimedes' principle and measuring the buoyancy of a polished glass sample in CCl_4. DTA and dilatometry measurements were carried out to obtain values for the thermal properties, T_g and α.

3. Results

3.1. UV absorption

Fig. 1a shows vacuum UV transmission spectra of an undoped borosilicate (BS) glass sample with high

Table 1. Batch compositions and some properties measured on un-doped basic glass samples investigated.

Glass	Composition (mol%)	$T_g \pm 5$ (°C)	Thermal coefficient α 100–300 °C (10^{-7} K^{-1})	Density ϱ (g cm^{-3})	Refractive index n_e	Dispersion coefficient ν_e	VUV edge λ_0 (nm)
Fluoride FP	$35\ AlF_3 - 15\ SrF_2 - 30\ CaF_2 - 10\ MgF_2 - 10\ Sr(PO_3)_2$	440	160	3.50	1.4601	90	160
Phosphate P	$50\ P_2O_5 - 50\ SrO$	495	125	3.20	1.5614	66	170
Borosilicate BS	$82\ SiO_2 - 12\ B_2O_3 - 1\ Al_2O_3 - 5\ Na_2O/K_2O$	530	33	2.22	1.4733	66	175

purity (analysed Fe content < 1 ppm) and two samples doped with 20 ppm iron melted under reducing and oxidising conditions. Fig. 1b demonstrates the fit of two charge-transfer bands for Fe^{3+} with Gaussian shape. The dominating band has a maximum at 222 nm (45 000 cm^{-1}) and a very large bandwidth (full width at half maximum), 11 000 cm^{-1}. But a second smaller band (width ~5500 cm^{-1}) with a maximum at 255 nm (39 200 cm^{-1}) with lower intensity was necessary for a well fitting of all measured spectra of the iron-doped glass samples melted under oxidising conditions. Fe^{2+} could not be detected in this sample with an error lower than 10% . On the contrary, large amounts of Fe^{3+} were found (15 to 70%) in all doped BS samples melted under reducing conditions. Fig. 1c illustrates a typical fit of one charge transfer band of Fe^{2+} with a maximum at 215 nm (46 500 cm^{-1}) and a small band width, ~5500 cm^{-1}, besides the two bands for Fe^{3+}. In comparison with the analysed Fe content by ICP–OES, chemical analysis and the fitted optical absorption spectra, the specific absorption coefficients for Fe^{3+} and Fe^{2+} in the borosilicate glass matrix (BS) were determined and compared with those in phosphate (P) and fluoroaluminate (FP) samples from previous papers [3, 4, 11, 12, 20] (Table 2).

Figs. 2–4 show the vacuum UV spectra of undoped and Sn doped glass samples investigated and possible fits for a $d \rightarrow s$ transition of Sn^{4+} with a maximum near the intrinsic VUV edge besides $s \rightarrow p$ transitions for Sn^{2+}, which were found in all tin doped samples with high accuracy. In fluoroaluminate (FP) and phosphate (P) glass samples doped with tin, the electronic transitions of tin ions detected by optical absorption and luminescence spectroscopy are shifted to shorter wavelength, that means higher energies (Figs. 2 and 3). The amounts of Sn^{4+} and Sn^{2+} depending on the host glass were estimated by Mössbauer spectroscopy [21]. The values obtained are summarised in Table 3.

3.2. UV-radiation-induced effects in iron-doped glass samples

Fig. 5 demonstrates the typical effect of photo-oxidation of Fe^{2+} by UV lamp irradiation in fluoride glass samples melted under reducing conditions, FP with ~15 ppm Fe^{2+}, on UV transmission (**a**), and the kinetic curves (**b**) depending on exposure time with increasing phosphate content. No change of Fe^{3+} species could be detected by UV irradiation of fluoride and phosphate glass samples [4], in contrast to silicate glass samples.

Fig. 6 shows the maximal defect formation curves by different UV lamp irradiation in iron-doped borosilicate glass samples melted under reducing (**a**) or oxidising (**b**) conditions. The influence of 193 nm laser irradiation with increasing pulse energy density on BS glass samples with 20 ppm Fe is given in Fig. 7. The kinetic curves are very different, depending on reducing (Fig. 7a) or oxidising (Fig. 7b) melting conditions. Figs. 8a and b illustrate the fitting procedure used in comparison with EPR [20] analysis in iron doped BS glass samples. Nearly 10 ppm $(Fe^{2+})^+$ hole centre and mainly boron-related electron centre defects were attributed in samples melted under oxidising conditions (Fig. 8a). Approximately 6 ppm $(Fe^{3+})^-$ electron centre combined with boron–oxygen related hole centre (BOHC) and also boron-related electron centre defects (B-EC) were found in samples melted under reducing conditions (Fig. 8b).

Figs. 9–13 give an overview of the UV lamp and laser-radiation-induced defects in different tin-doped glass samples. Tin-doped fluoroaluminate glass samples, FP/50 ppm Sn as Sn^{2+}, are very stable against UV lamp irradiation. No significant change of the tin absorption was detected in fluoride glass samples, only photo-oxidation of ~3 ppm Fe^{2+} from the initial value, $[Fe^{2+}]_0 \sim 15$ ppm, as impurity (Fig. 9a and b). In contrast to phosphate, $Sr(PO_3)_2$/50 ppm Sn with ~35 ppm as Sn^{2+} and Fe' < 5 ppm, and borosilicate glass samples, BS/200 ppm Sn with ~30 ppm as Sn^{2+} and ~170 ppm as Sn^{4+}, in which strong decrease of Sn^{2+} absorption also occurs with UV lamp irradiation. In FP glass samples with ~50 ppm Sn^{2+}, tin defect generation was found only with 193-nm excimer laser irradiation, which correlates with a very high negative radiation-induced absorption < 200 nm and positive values > 200 nm (Fig. 10). Defect formation at 193 nm is typical for Sn^{2+}-related defects and
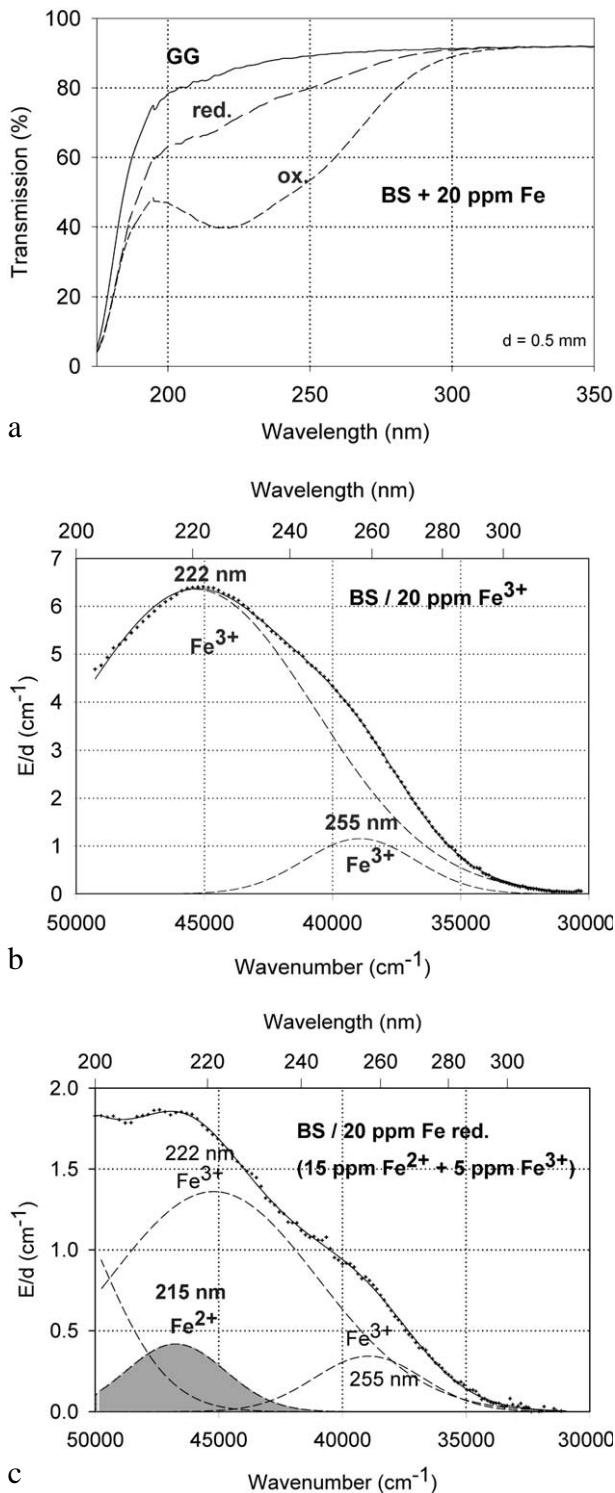
a

b

c

Fig. 1. Influence of iron on the ultraviolet absorption of high-purity borosilicate glass samples, BS. (**a**) Vacuum ultraviolet transmission spectra of BS glass samples doped with 20 ppm Fe melted under oxidising (ox) and reducing (red) conditions in comparison with an undoped sample (GG) with an analysed Fe content < 1 ppm. (**b**) Peak simulation for 20 ppm Fe^{3+} (sample ox) with two Gaussian bands (dashed lines). The measured data (pointed line) could be well fitted (line). No Fe^{2+} was detectable. (**c**) Peak simulation for the sample with 20 ppm Fe (red). One Gaussian band for Fe^{2+} with a maximum at 215 nm was found besides the two bands for Fe^{3+}.

at 450 nm for phosphorus oxygen-related hole-centre defects (POHC).

Fig. 11 compares the tin related defect formation in $Sr(PO_3)_2$/50 ppm Sn glass samples by different laser irradiation wavelength at 193 and 248 nm. Defect formation at ~196 nm is typical for Sn^{2+}-related defects and at ~500 nm for POHC defects, which are much higher with 193-nm than with 248-nm laser irradiation. Figs. 12 and 13 give an overview of typical UV-radiation-induced defects in borosilicate glass samples doped with 200-ppm tin. The influence of 248-nm laser irradiation depending on pulse number and energy density per pulse is shown. At high energy density, 350 mJ cm^{-2} per pulse, a very fast change of the UV transmission in a opposite way is observed already after 100 pulses: an increase of the transmission below ~230 nm and a decrease between 230 and 400 nm. At further irradiation, the increase of transmission < 230 nm is continued slowly, but for wavelengths > 230 nm, an increase in transmission is also found (Fig. 12a). The kinetic curves for the typical defect formation, depending on the pulse number and energy density per pulse, are demonstrated at $\lambda = 206$ nm, as the maximum of the Sn^{2+} absorption, in Fig. 12b, and at $\lambda = 250$ nm, in Fig. 12c. The defect generation at 250 nm increases very fast, in the same way as the Sn^{2+} absorption decreases, reaches a maximum after ~100 pulses, but then, after further irradiation, this defect generation decreases again. Both effects increase with increasing energy density. Figs. 13a, b and c show a first assumption of a peak simulation for the 248-nm laser-induced defect generation at the highest energy density, 350 mJ cm^{-2} per pulse. The measured data (lines) could be well fitted with Gaussian functions (dashed lines) with a correlation coefficient > 0.999, and in good agreement with EPR measurements. After 100 pulses, the Sn^{2+} absorption bands are decreased and a lot of bands, accordingly EPR measurements mainly boron-related EC and HC defects, are formed, Fig. 13(a). Between 100 and 5000 pulses, further decrease of the Sn^{2+} bands connected with an increase of the boron-related defect bands is observed (Fig. 13b). As a result, after 5000 pulses (Fig. 13c), only a few weak intrinsic bands with maximums at 255, 280 and 340 nm besides the strong negative Sn^{2+} bands could be detected.

In the EPR spectra of tin-doped BS glass samples three additional signals, with g-values at 1.9775, 1.9866 and 1.9977, were found in all irradiated samples. The nature of these defects is still unknown, but their intensity was increased with increasing tin content.

Table 2. Charge transfer bands and specific extinction coefficients ε_λ for Fe^{3+} and Fe^{2+} complexes in different host glasses.

Glass	Fe^{3+}					Fe^{2+}				
	λ_{max} (nm)	Energy		$\varepsilon_\lambda (cm^{-1} ppm^{-1})$	Width (cm^{-1})	λ_{max} (nm)	Energy		$\varepsilon_\lambda (cm^{-1} ppm^{-1})$	Width (cm^{-1})
		(cm^{-1})	(eV)				(cm^{-1})	(eV)		
Fluoride	185	55 500	6.9	0.25 ± 0.05	6000	170	58 800	7.3	0.20 ± 0.05	5000
FP	260	38 500	4.8	0.18 ± 0.02	8000	220	45 500	5.6	0.006 ± 0.001	4000
Phosphate	240	41 700	5.3	0.20 ± 0.01	10 000	~220	~45 500	5.6	< 0.01	~6000
P										
Borosilicate	222	45 050	5.6	0.30 ± 0.02	11 000	215	46 500	5.8	0.03 ± 0.01	5500
BS	255	39 200	4.9	0.06 ± 0.01	5500					

a

b
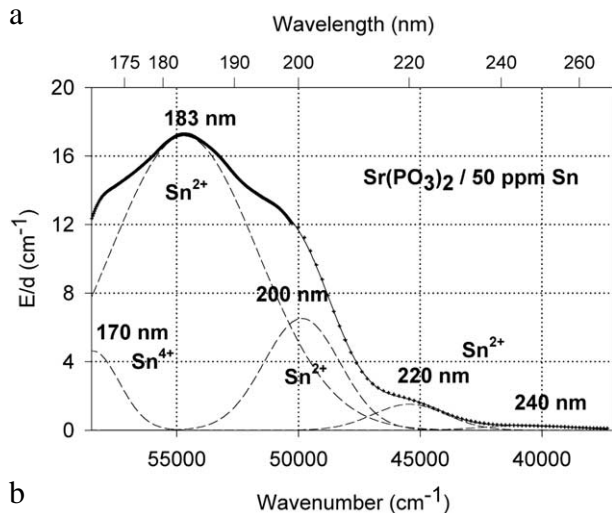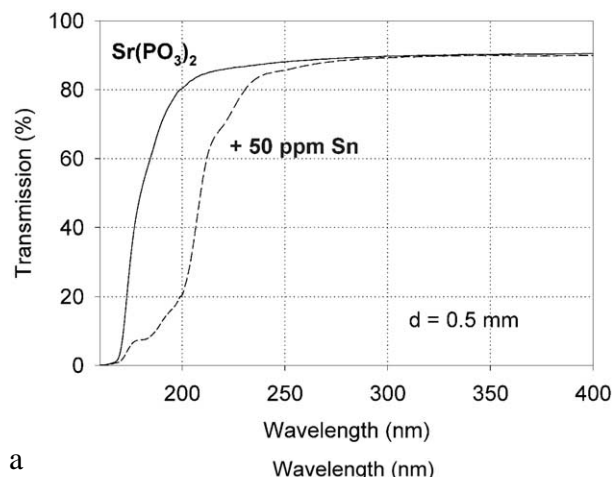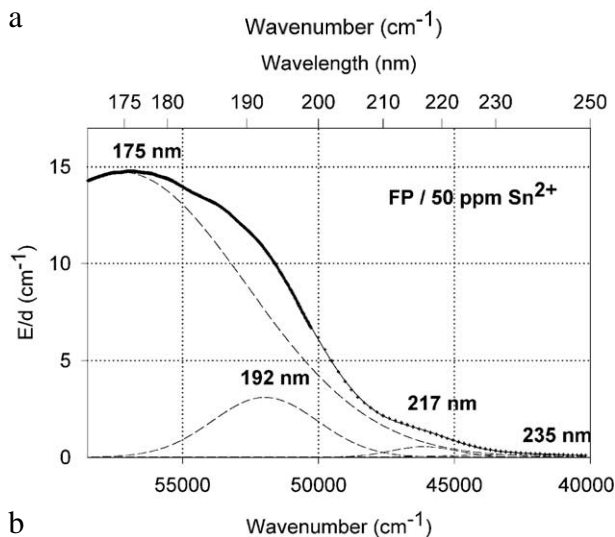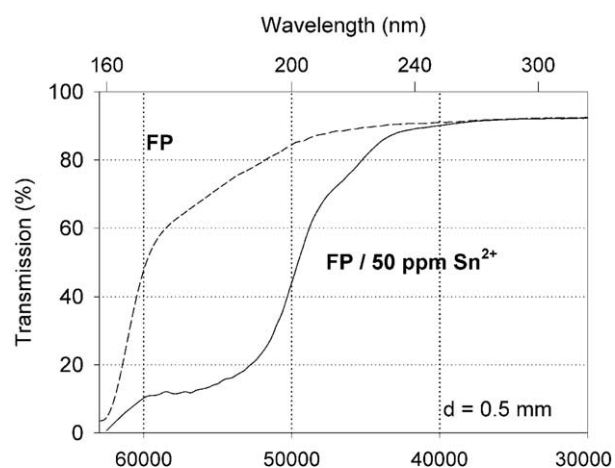
Fig. 2. Influence of tin on the ultraviolet absorption of fluoroaluminate glass samples, FP, melted under reducing conditions. (**a**) Vacuum ultraviolet transmission spectra of FP glass samples with 15 ppm Fe^{2+} and additional doped with 50 ppm Sn as Sn^{2+}, analysed ~30 ppm. (**b**) Peak simulation for s → p electronic transitions of Sn^{2+} in the FP glass sample with four Gaussian bands (spectra of tin doped minus un-doped glass sample). The dominating band has its maximum in the vacuum ultraviolet region at 175 nm. The absorption > 200 nm is very weak.

a

b

Fig. 3. Influence of tin on the ultraviolet absorption of phosphate glass samples, P, melted under normal conditions. (**a**) Vacuum ultraviolet transmission spectra of P glass samples with < 5 ppm Fe' and additional doped with 50 ppm Sn, ~ 35 ppm as Sn^{2+} and ~ 15 ppm as Sn^{4+}. (**b**) Peak simulation for s → p electronic transitions of Sn^{2+} with four Gaussian bands and one for a possible d → s transition of Sn^{4+}, overlapping with intrinsic VUV edge, in the P glass sample (spectra of tin doped minus un-doped glass sample). The dominating band has its maximum in the vacuum ultraviolet region at ~180 nm. The absorption > 200 nm is also very weak, but stronger than in the FP glass sample (Fig. 2).
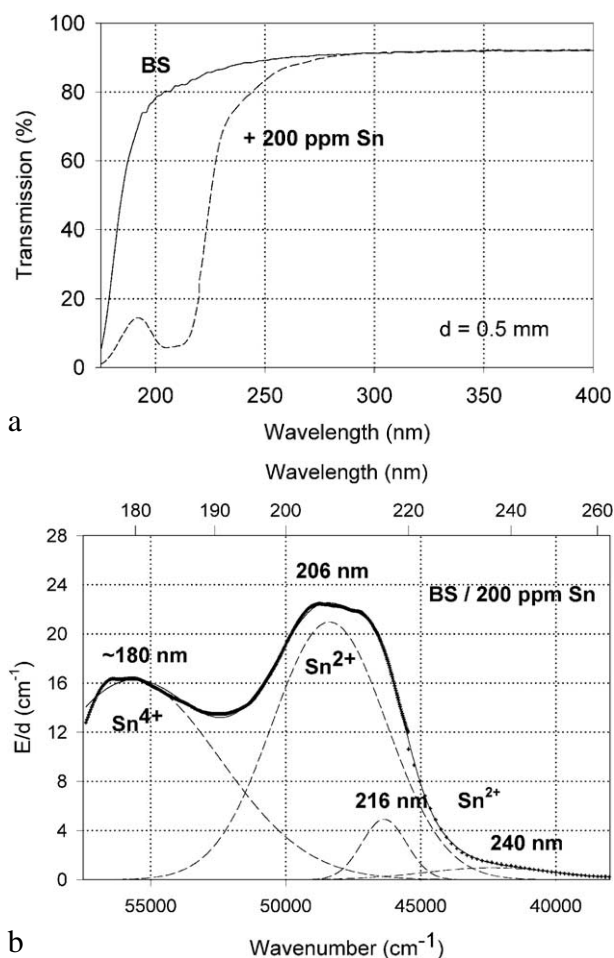
a

b

Fig. 4. Influence of tin on the ultraviolet absorption of high-purity borosilicate glass, BS. (**a**) Vacuum ultraviolet transmission spectra of a borosilicate glass sample, BS, doped with 200 ppm Sn in comparison with the undoped sample (Fe < 1 ppm). (**b**) Peak simulation with Gaussian bands (dashed lines). Three bands for Sn^{2+} were well fitted in all Sn doped samples with very high accuracy. A fourth band with a maximum at 260 nm was detectable at higher tin concentration. Additionally, one band for Sn^{4+} was necessary, with a maximum near the intrinsic band edge. After Mössbauer measurements [21], only 10–15% tin should exist in the Sn^{2+}(~30 ppm) and 85-90% in the Sn^{4+} state (~170 ppm).

4. Discussion

4.1. Charge transfer absorption of Fe^{3+} and Fe^{2+} complexes in different glasses

The three glass types investigated (Table 1) have very low optical basicity, Λ [10], and a large intrinsic UV transmission. But their structure is very different [4, 5] and so their influence on charge transfer absorption of Fe^{3+} and Fe^{2+} complexes is also different. The dominating UV absorption bands are caused in all three glass types by Fe^{3+} complexes. The measured spectra could be well fitted with Gaussian shape bands. In the fluoride phosphate glass FP with the
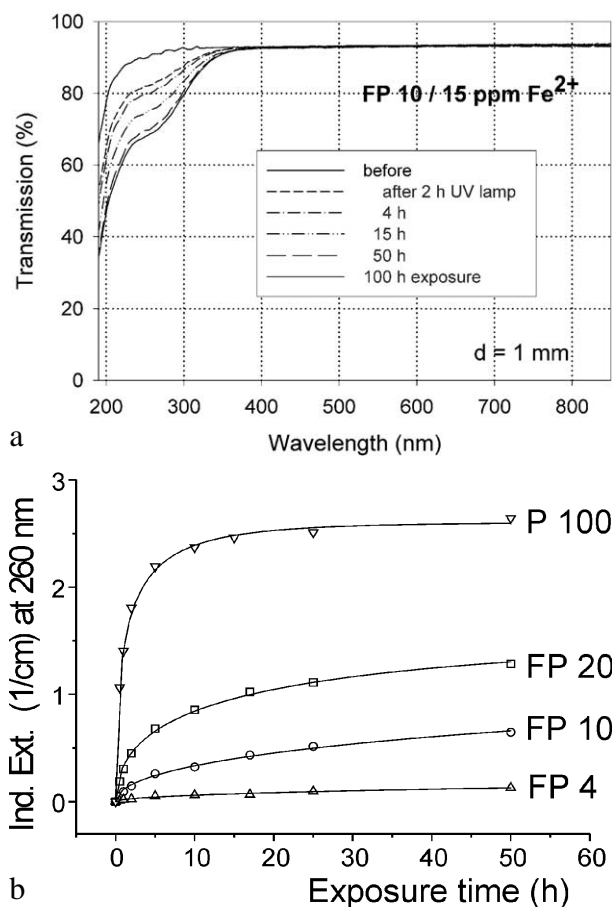

a

b

Fig. 5. Photo-oxidation of Fe^{2+} to $(Fe^{2+})^+$ in fluoroaluminate glass samples by UV lamp irradiation. (**a**) Change in transmission by UV lamp irradiation after different exposure times. (**b**) Kinetic curves as a function of increasing phosphate content (4–10–20 mol%) in FP glass samples in comparison with a pure phosphate glass sample (P 100). The initial Fe^{2+} content in all of the glasses was nearly the same (~15 ppm). The continuous curves denote the function (1), which is fitted to the experimental data. The error of the measured points is < 0.01 cm^{-1}.

lowest optical basicity, $\Lambda_{Pb} = 0.38$, and the highest ionic bonding, the band maximum, $\lambda = 260$ nm, has the lowest energy (38 500 cm^{-1} = 4.8 eV), the smallest bandwidth (8000 cm^{-1}), and the lowest specific absorption coefficient, $\varepsilon_{260\,nm} = 0.18$ cm^{-1} ppm^{-1}. The charge transfer should occur from the surrounding ligands to the central Fe^{3+} ion. In the case of FP, ligands are mainly fluorine in six-fold coordination, but oxygen ligands are possible too. The charge-transfer process in glass can be regarded as the promotion of a nonbonding p electron, on the ligand, to the lowest unoccupied energy orbital sited on the metal ion [10].

In phosphate glasses, $Sr(PO_3)_2$ and ultraphosphate [4], the maximum for the Fe^{3+} charge transfer band ($\lambda = 240$ nm) is shifted to a higher energy (41 700 cm^{-1} = 5.2 eV), a higher intensity (ε_{240nm}
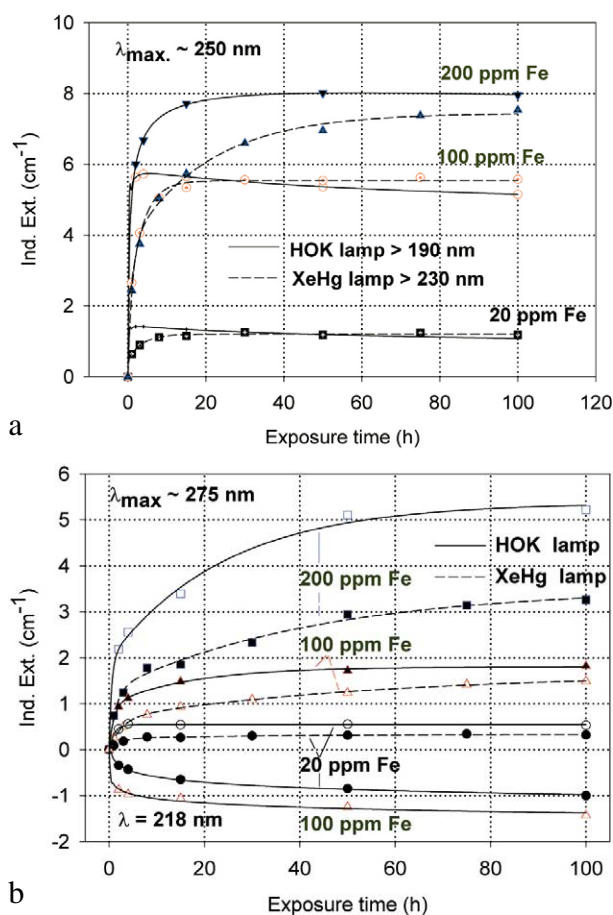
a

b

Fig. 6. Kinetic curves for the maximal defect generation by different UV lamp irradiation, HOK ($\lambda < 190$ nm) and XeHg ($\lambda < 230$ nm) lamp, of borosilicate glass samples doped with increasing iron content, 20–200 ppm. (**a**) Samples melted under reducing conditions: the defect generation at $\lambda_{max} \sim 250$ nm increases very fast with iron content, especially with the HOK lamp. The continuous curves denote the function (2) for the HOK and (3) for the XeHg lamp, which are fitted to the experimental data. (**b**) Samples melted under oxidising conditions: a significant negative induced absorption at $\lambda \sim 218$ nm is observed only with HOK irradiation in samples doped with 20 and 100 ppm Fe. Their continuous curves denote the function (4), which is fitted to the experimental data. The positive induced absorption at $\lambda_{max} \sim 275$ nm increased with the Fe content; it is also stronger with the HOK than with the XeHg lamp. Their continuous curves denote the function (3) for both lamps.
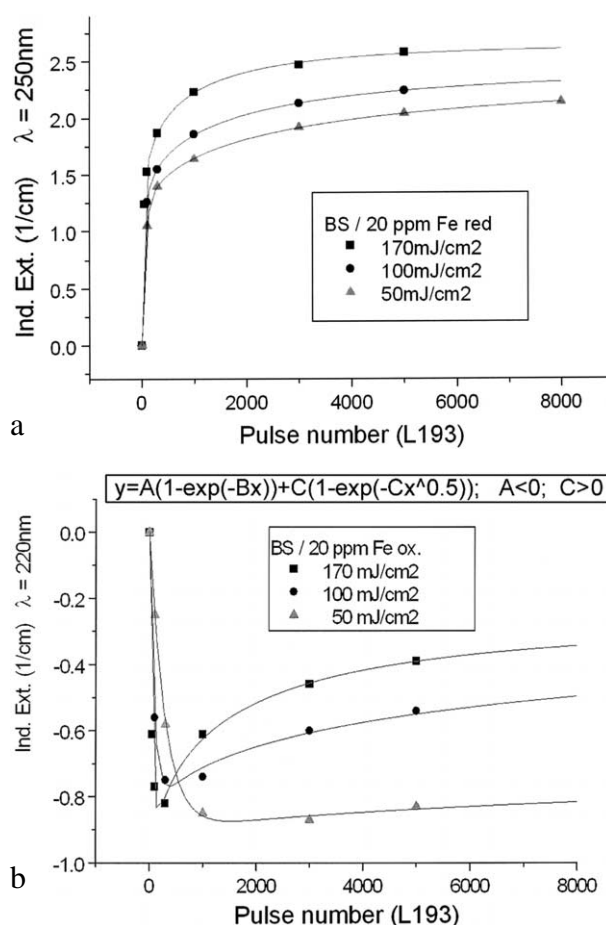

a

b

Fig. 7. Kinetics for ArF laser defect generation in borosilicate glass samples with 20 ppm Fe melted under (**a**) reducing and (**b**) oxidising conditions, depending on pulse energy density: (**a**) at $\lambda = 250$ nm, depending on pulse number, a very fast increase of the defect generation with increasing energy density per pulse is observed; (**b**) at $\lambda = 220$ nm at first, a very fast negative induced absorption is observed, but after more than 100 pulses, this effect goes back, especially at high energy density, 170 mJ cm²; at low energy density, 50 mJ cm⁻², the rate of increase is only small. All continuous curves denote the function (5), which is fitted to the experimental data.

$= 0.20$ cm⁻¹ ppm⁻¹) and a larger bandwidth (10 000 cm⁻¹). These phosphate glasses possess a higher optical basicity, $\Lambda_{Pb} = 0.47$, and a higher covalent bonding than the FP glass.

The borosilicate glass (BS ~ Duran) with nearly the same low calculated optical basicity [20], like the phosphate glass, shows another behaviour for the Fe^{3+} charge-transfer bands, due to other sites for Fe^{3+}. A very strong and broad band with a maximum at 222 nm (45 050 cm⁻¹ = 5.6 eV) is dominating (Fig. 1) and in good agreement with the data in high-purity

soda–silica glass [13]. A very high specific absorption coefficient, $\varepsilon_{222nm} = 0.30$ cm⁻¹ ppm⁻¹, was determined. But a second smaller band with a maximum at 255 nm with lower intensity ($\varepsilon_{255nm} = 0.06$ cm⁻¹ ppm⁻¹) was necessary for a well fitting of all measured spectra of iron doped BS glass samples. These Fe^{3+} charge transfer bands could be determined in all glasses investigated with high accuracy [2–4]. Further transitions for Fe^{3+} and Fe^{2+} are assumed near the intrinsic UV edge of the glasses (Fig. 1a).

Exact determination of the Fe^{2+} charge transfer bands is more difficult. Only in FP glasses was it possible to shift the redox ratio completely to the Fe^{2+} state [2–4, 12, 20] and to determine the bands with high accuracy (Table 2). However, in phosphate and
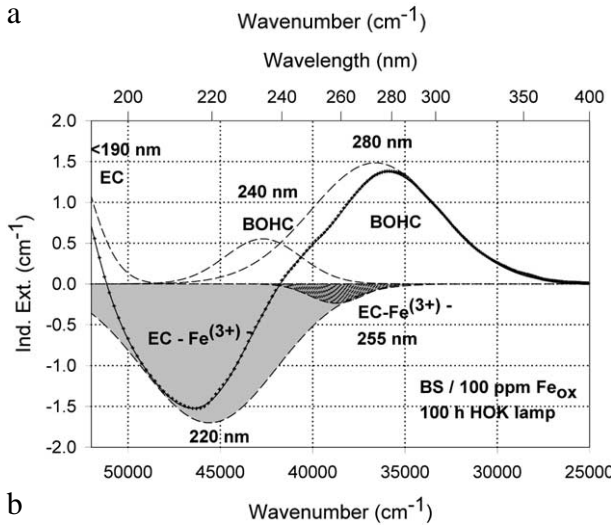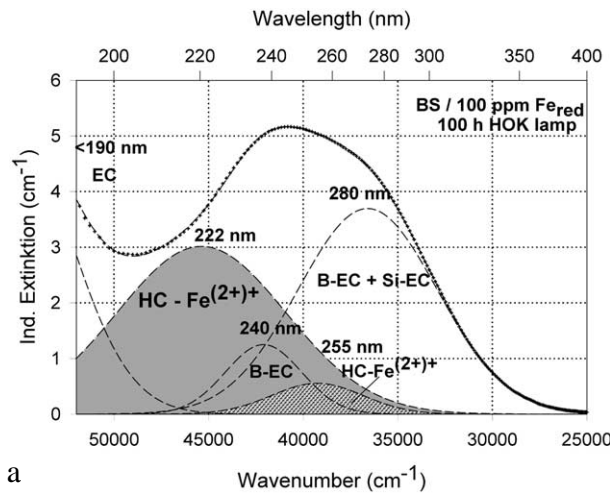
685

Fig. 8. Peak simulation and designation of defect bands in BS samples with 100 ppm Fe after 100-h HOK lamp irradiation: (**a**) sample melted under reducing conditions; (**b**) sample melted under oxidising conditions.
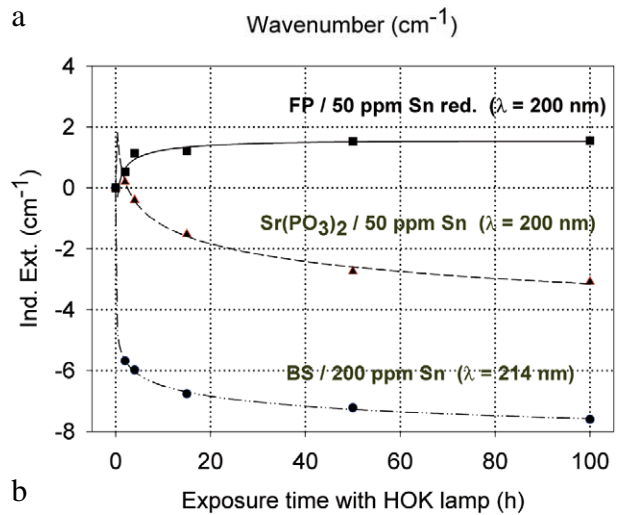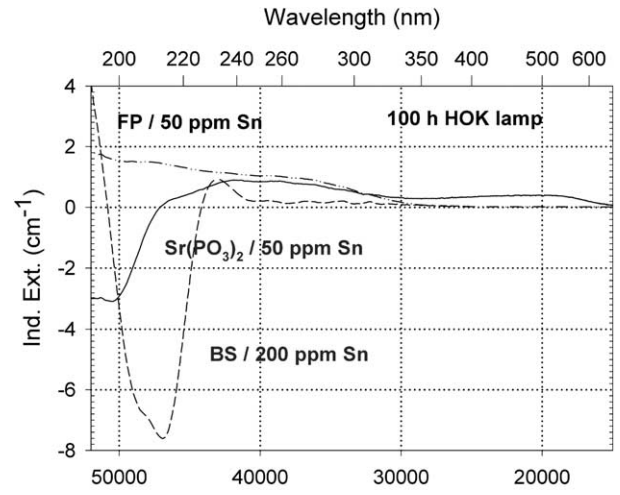

Fig. 9. Comparison of UV-lamp-radiation-induced absorption in different tin doped glasses with nearly the same initial Sn^{2+} content, ~30 ppm. (**a**) Negative induced absorption in the region of Sn^{2+} electron transitions was found only in the phosphate and boro-silicate glass samples. No significant change in the tin absorption was detected in fluoride glass samples, only photo-oxidation of ~3 ppm Fe^{2+} from the impurity. (**b**) Kinetic curves for the maximal defect generation. Their continuous curves denote the function (2), which is fitted to the experimental data.

silicate glasses, the values for the Fe^{2+} charge transfer bands determined have a larger error. The main band maximum is between 215 and 220 nm, with a much lower intensity (ε_λ: 0.006 to 0.03 $cm^{-1}\ ppm^{-1}$) than those for Fe^{3+}.

4.2. Electronic transitions for Sn^{2+} and Sn^{4+}

Three or four electronic $s \rightarrow p$ transitions for Sn^{2+} with $5s^2$ configuration were detected by optical absorption and luminescence [20, 22] spectroscopy shifted to longer wavelength in the range $FP \rightarrow P \rightarrow BS$ glass samples with increasing covalent bonding (Table 3). These electronic transitions are parity allowed and depends strongly from the host glass (Figs. 2–4). Three transitions could be well fitted in glass samples with only a few ppm Sn^{2+} (Figs. 2b and 3b); with higher Sn^{2+} content, a fourth band at longer wavelength was found (Table 3). The highest

intensity should have the allowed $^1S_0 \rightarrow {}^1P_1$ transition with a maximum at ~175 nm in FP, ~180 nm in P and at 206 nm in BS glass samples. The $^1S_0 \rightarrow {}^3P_2$ is forbidden ($\Delta J = 2$), but can obtain some intensity by coupling with vibrations, assuming for the fitted band with a maximum at 192 nm in FP, at 200 nm in P and at 216 nm in BS glasses. A third band, with a maximum at 217 nm in FP, at 220 nm in P and at 240 nm in BS samples and low intensity was fitted assuming for the $^1S_0 \rightarrow {}^3P_1$ transition, which is spin-forbidden but can also be observed, due to spin-orbit coupling, which mixes the spin triplet and singlet states [20, 22]. The intensity ratios detected for the four transitions in all tin-doped glass samples investigated were
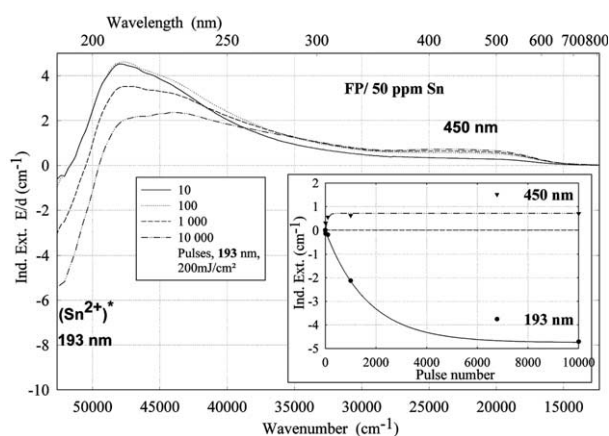
Fig. 10. ArF (193 nm)-laser-radiation-induced absorption in a tin-doped FP glass sample depending on pulse number, energy density per pulse: 200 mJ cm^{-2}; the continuous kinetic curves denote the function (6), which is fitted to the experimental data.
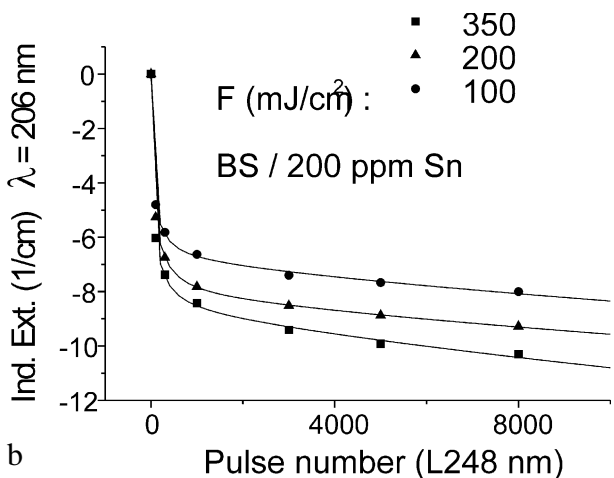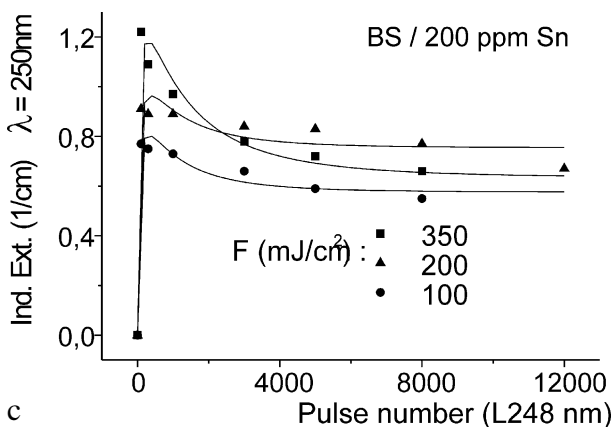

Fig. 11. Comparison of laser-radiation-induced absorption in tin-doped phosphate glass samples for different laser wavelengths (with the same energy density per pulse: 200 mJ cm^{-2}): (**a**) ArF laser at 193 nm, (**b**) KrF laser at 248 nm. The continuous kinetic curves denote the function (6), which is fitted to the experimental data.
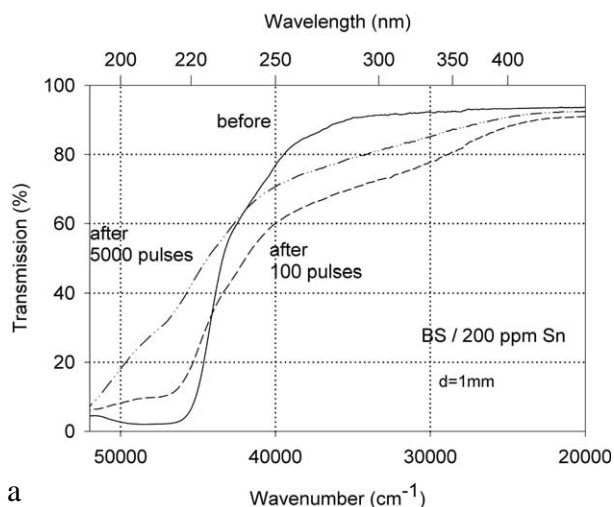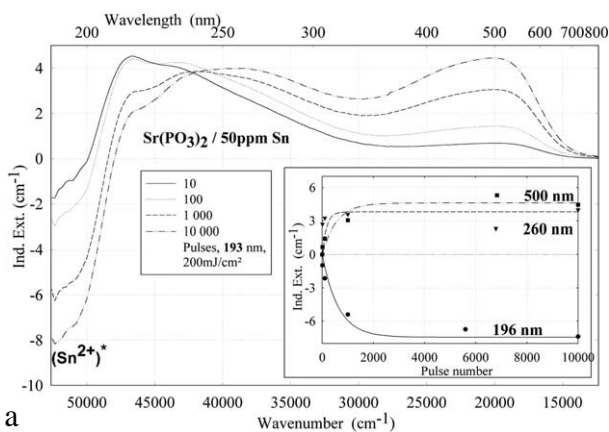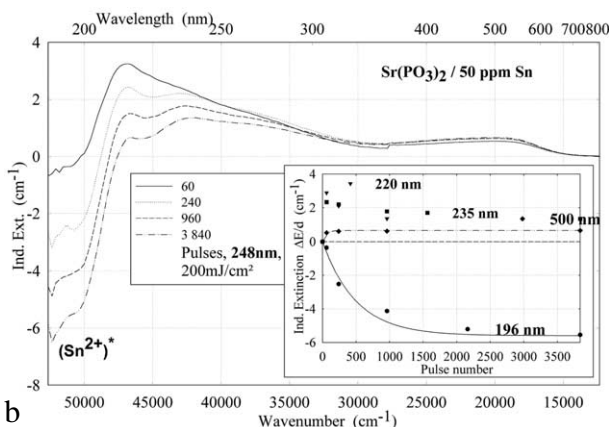
Fig. 12. Influence of laser irradiation at 248 nm (KrF) on BS glass samples with 200 ppm Sn (~30 ppm as Sn^{2+}): (**a**) UV transmission spectra before and after laser irradiation with a pulse energy density, 350 mJ cm^{-2}; (**b**) defect formation at 206 nm, depending on energy density and pulse number typical for Sn^{2+} related defects; (**c**) defect formation at 250 nm, depending on energy density and pulse number typical for intrinsic defects.
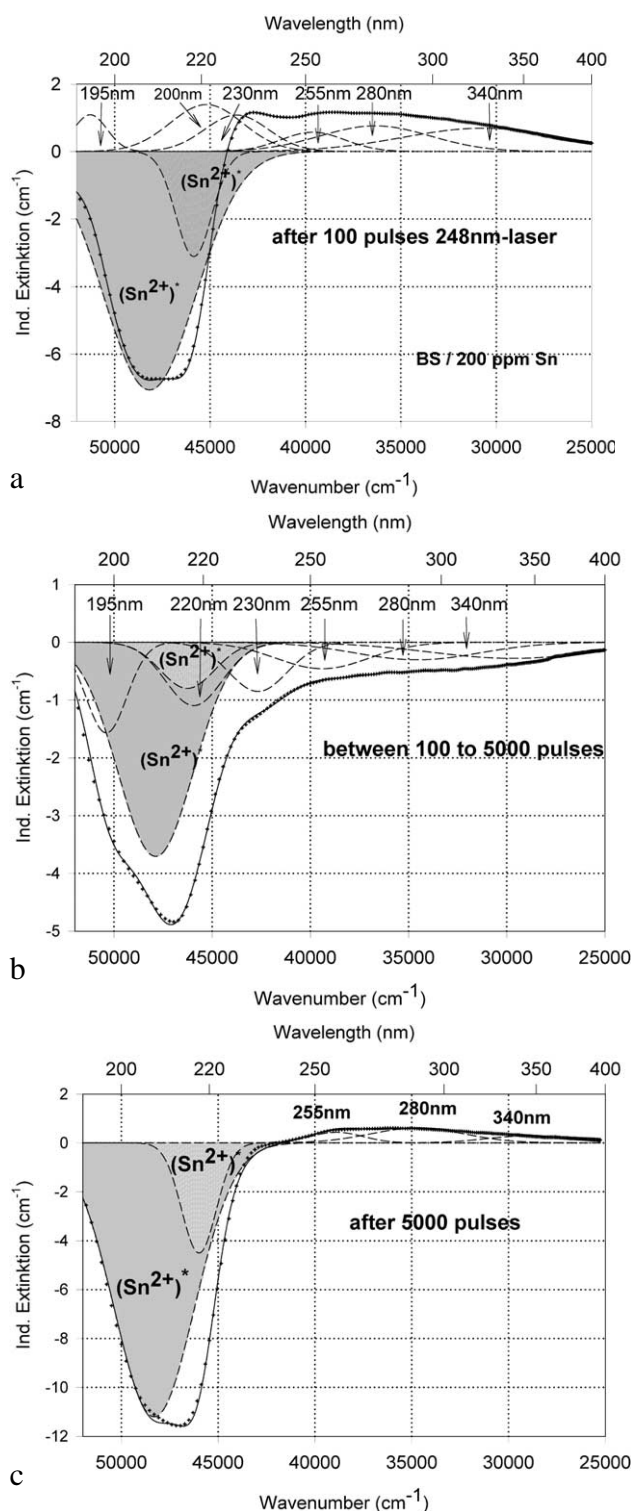
Fig. 13. Peak simulation for the induced defects by 248-nm laser irradiation at high energy density, 350 mJ cm^{-2} per pulse (see Fig. 12): (**a**) after 100 pulses; (**b**) between 100 and 5000 pulses; (**c**) after 5000 pulses.

approximately 10:5:1:0.1. The specific absorption coefficients, ε_λ, were calculated with chemical analysis, absorption and luminescence spectroscopy and

Mössbauer measurements on samples doped with higher tin contents (0.5–1%) and melted under the same conditions [21]. Only 10–15% of the total tin content was found in the Sn^{2+} state in BS samples. The extrapolation to very low Sn concentration is still a problem, and so the absolute values for the absorption coefficients are not so sure.

In the case of FP and P glasses, the Sn^{4+}/Sn^{2+} ratio could be completely shifted to Sn^{2+} by melting under reducing conditions in a carbon crucible at temperatures > 1000 °C [21]. The s → p transitions are shifted in the vacuum UV region (Figs. 2 and 3) and these measurements have a larger error (~30%) (Table 3).

For the Sr(PO$_3$)$_2$ glass sample doped with 50 ppm Sn, exists only an estimated value of ~30 ppm Sn^{2+}. The Sn^{2+} luminescence excitation and emission spectra [20] are also strongly dependent on the host glass. Narrow bands were measured in BS and very broad bands in FP samples different from those in P samples, due to the influence of the various local structure (surrounding ligands). But all measured spectra could be also well fitted with three or four Gaussian bands.

In all glasses investigated, a d → s electronic transition band with low intensity for Sn^{4+} in the VUV was found overlapped with the intrinsic edge (Table 3).

4.3. Radiation-induced effects in iron doped glasses

The influence of iron on radiation-induced effects in phosphate and fluoride phosphate glasses was described in previous papers [2, 4, 14, 15]. Photo-oxidation of Fe^{2+}, forming (Fe^{2+})$^+$ hole centres (HC) and phosphorous related electron centres (EC) as a single photon process, was found with UV-lamp and laser irradiation in both glass types, phosphates (ultra- and meta-phosphates) and fluoride phosphates melted under reducing conditions (Fig. 5a and b). But the time dependence to reach the saturation value, for which a maximum of 50% of the initial Fe^{2+} content has been photo-oxidised, was very different. The measured kinetic curves could be well fitted with the function:

$$f(t) = A[1 - \exp(-B\,t^{1/2})] \qquad (1)$$

where A and B are constants. A is the saturation value, i.e. the limiting amount of the photo-oxidised (Fe^{2+})$^+$, and is directly proportional to the initial Fe^{2+} content; B correlates with the energy density of the lamp radiation. In FP glasses, the time for reaching the saturation value increases drastically with increasing phosphate content (with HOK-lamp irradiation ~100 000 h in FP 4, 1200 h in FP 10 and 100 h in FP 20); the shortest time of 15 h was found in the

Table 3. Absorption bands and specific extinction coefficients ε_λ for Sn^{2+} and Sn^{4+} complexes in different host glasses.

| Glass | Sn^{2+} | | | | | Sn^{4+} | | | | |
| | λ_{max} (nm) | Energy | | ε_λ (cm⁻¹ ppm⁻¹) | Width (cm⁻¹) | λ_{max} (nm) | Energy | | ε_λ (cm⁻¹ ppm⁻¹) | Width (cm⁻¹) |
		(cm⁻¹)	(eV)				(cm⁻¹)	(eV)		
Fluoride FP	175	58 000	7.3	0.4 ± 0.1	11 000	< 170	>58 000	>7.3		
	190	52 600	6.5	0.2 ± 0.1	5000					
	217	46 000	5.7	0.02 ± 0.01	3000					
	235	42 300	5.2	~ 0.002	6000					
Phosphate P	~185	~54 000	~6.9	0.4 ± 0.1	~6000	~170	~58 000	~7.3		
	200	50 000	6.2	0.2 ± 0.1	4000					
	220	45 500	5.6	0.05± 0.1	4000					
	240	41 700	5.2	~ 0.005	5000					
Borosilicate BS	206	48 500	7.0	0.5 ± 0.2	5400	~180	~56 000	6.9	~0.1	~8000
	216	46 300	5.7	0.2 ± 0.1	2200					
	240	41 700	5.2	0.04 ± 0.01	5600					
	260	38 500	4.8	~ 0.005	6000					

phosphate glass without fluoride, P 100. The saturation value for $(Fe^{2+})^+$ concentration was found independent of the energy density of the UV lamp or laser, contrary to the time to reach it.

High-purity borosilicate glass samples, BS, with Fe < 10 ppm, are very stable against UV-lamp and 248-nm laser irradiation [6, 20]. Therefore, the formation of UV-radiation-induced defects increases drastically with increasing iron content, especially in samples melted under reducing conditions (Figs. 6–8). BS samples for technical use normally have an impurity content of 100 to 200 ppm Fe. These glasses melted under reducing conditions have a good transmission in the UV–B region (280–320 nm) but unfortunately also a high solarisation (Fig. 6a and b), which increases with shorter wavelength irradiation (HOK > XeHg lamp). The kinetic curves for the maximal defect generation in Fe-doped BS samples melted under reducing conditions at $\lambda_{max} \sim 250$ nm (Fig. 6a) could be well fitted with the following functions:
– for HOK-lamp irradiation

$$y = y_0 + a \ln x + b (\ln x)^2 + c (\ln x)^3 \quad (2)$$

– for XeHg-lamp irradiation

$$y = y_0 + a [1 - \exp(-b x)] + c [1 - \exp(-d x)] \quad (3)$$

In the case of samples melted under oxidising conditions (Fig. 6b), the maximal positive defect generation at $\lambda_{max} \sim 275$ nm, depending on the exposure time x, could be fitted for both lamps with the same function (3), and for the negative defect generation at $\lambda_{max} \sim 218$ nm with a simpler function (4):

$$y = y_0 + a \ln x \quad (4)$$

This means that the mechanisms for the radiation-induced processes are very difficult to recognise, because they are very complex. The defects can change. With HOK and laser irradiation, the formation

curves can pass through a maximum or a minimum, due to change of photo-oxidation into photoreduction of the iron species, which is strongly dependent on the irradiation wavelength and the energy density (Figs. 6a and 7b). This makes the extrapolation of the defect generation for long-time irradiation very difficult, but increases the defect generation in silicate glasses with increasing iron content generally. Most kinetic curves can be well fitted with the function:

$$y = A [1 - \exp(-B x)] + C [1 - \exp(-C x^{1/2})] \quad (5)$$

with $A < 0$ and $C > 0$.

The designation of the generated defect was assumed by correlation of the induced optical bands, EPR analysis combined with thermal annealing experiments [20]. It was found that photo-oxidation of Fe^{2+} is the first dominating step in all samples melted under reducing conditions. That means Fe^{2+} absorbs an UV photon and loses an electron to form stabilised $(Fe^{2+})^+$ defect hole centres. The electron is trapped, forming boron- and silicon-related electron centres (Fig. 8a and b). The maximum for the induced $(Fe^{2+})^+$–HC absorption band is at the same position as that for the Fe^{3+} charge-transfer transition, at 222 nm (Fig. 8a). The fitted maximums for boron- and silicon-related EC are assumed at 240 and 280 nm. In BS glass samples with low alkali contents, boron-related EC defects dominate. The superposition of the induced bands leads to a maximal radiation-induced absorption at ~250 nm. The photo-oxidation rate is very high and increases with the energy density and the excitation efficiency for the Fe^{2+} species. The last is higher for the HOK, $\lambda > 190$ nm, than for the XeHg lamp, $\lambda > 230$ nm. In samples doped with 100 or 200 ppm Fe, the saturation value is not reached after 100 h irradiation with the XeHg lamp (Fig. 6a). The fitting results have shown that only 15 to 40% of the initial Fe^{2+} content was photo-oxidised. With HOK

lamp irradiation, then an another process is initiated: the photoreduction of Fe^{3+}, forming a $(Fe^{3+})^-$ defect electron centre by electron trapping and a boron-related hole centre (BOHC, $\lambda_{max} \sim 280$ nm), and also a boron-related electron centre (B-EC, $\lambda_{max} \sim 240$ nm), was detected as the dominating process in all samples melted under oxidising conditions (Figs. 6b, 7b, and 8b). The total content of the photo-reduced $(Fe^{3+})^-$ is very low, only 5 to 10% of the initial Fe^{3+} content; e.g., in the sample, BS/20 ppm Fe_{ox}, a maximum of 2–3 ppm Fe^{3+} was reduced to $(Fe^{2+})^-$ by HOK or laser (248 nm) irradiation (Figs. 6b, 8a and b). No significant photoreduction could be detected with XeHg-lamp irradiation and course-selective excitation of photoelectrons, $\lambda > 230$ nm; the highest values were found with X-rays, for which an avalanche of electrons is released [20]. Irradiation with the 193-nm laser, near the UV edge [5, 16], generates also intrinsic defects of BS in the visible region and an efficient fast photoreduction of Fe^{3+} (Fig. 6b). The results of the optical spectroscopy were consistent with those of the EPR analysis [20], also for the Fe^{3+} signal at $g \sim 4.3$.

The initial reaction for the solarisation should be the release of an electron. In the case of oxidised melted samples, it is not clear where does this electron come from? High-purity BS samples, Fe < 1 ppm, are very stable against UV lamp and laser (248 nm) irradiation (Fig. 4), but solarisation increases with increasing the iron content. It could be also possible that traces of Fe^{2+} (< 10% of the total Fe content) in the oxidised samples are responsible for the first step, the release of an electron, as the initiator for the photoreduction of Fe^{3+}. But there has to be still an influence of the surrounding glass matrix, because this process was not found in fluoride and phosphate glasses [4, 14, 15, 17, 20]. In these glasses, Fe^{3+} species were not able to trap an electron and stabilise a $(Fe^{3+})^-$ defect electron centre. This is in contrast to the chemical reduction of Fe^{3+} to Fe^{2+} in the glass melt, which occurs very easy in FP and P systems [2–4]. In the melts, a relaxation of the local structure for stabilising the reduced species is possible, whereas in the glass at room temperature this relaxation is not possible. The Fe^{3+} complexes are very stable and not involved in radiation-induced processes. They can be used as filters for increasing the radiation resistance. This is the main difference between fluoride and phosphate glasses, on the one hand, and silicate and borosilicate ones, on the other hand; in these latter, both Fe^{2+} and Fe^{3+} species take part into UV-radiation-induced processes, due to the local glass structure.

The photo-oxidised $(Fe^{2+})^+$ defects in all glass samples investigated can also be formed with thermal treatment of irradiated glasses and no recovery was detected, in contrast to the photoreduced $(Fe^{3+})^-$ defects, which were annealed to Fe^{3+} by thermal treatment below the T_g temperature.

4.4. Radiation-induced effects in tin doped glasses

Tin doped FP glasses (Figs. 2a, 9a and b) are very stable against UV lamp irradiation, in comparison to tin-doped P and BS glasses. The HOK lamp spectrum starts at very short wavelengths, > 190 nm, for which an excitation of the Sn^{2+} electronic transitions is possible in all glasses investigated (Fig. 2–4). But, in FP glasses, no significant change in Sn^{2+} absorption bands with UV lamp irradiation was detected, but only photo-oxidation of Fe^{2+} as an impurity (Fig. 9a and b). This means that the fluoride glass structure prevents a tin-related defect generation by UV lamp irradiation. With 193-nm laser irradiation, pulse energy density 200 mJ cm^{-2}, a fast Sn^{2+}-related defect generation in FP glass samples was found (Fig. 10). The dependence of the measured kinetic curves on pulse number could be well fitted with the following equation (6):

$$f(x) = A \left[1 - \exp(-Bx^C) \right] \qquad (6)$$

where A and B depend on the energy per pulse, and the value of C depends on the doping agent. This dependence (6) allows the extrapolation of the saturation values A of the induced extinction for all tin doped samples investigated [6] (Figs. 10–13). Fig. 10 shows the saturation value at 193 nm in FP/50-ppm Sn glass samples with –5 cm^{-1}, due to photo-oxidation of Sn^{2+} species, which form hole centre defects. There should be built also electron centre defects that could be Sn^{4+}-species-trapped electrons. The defect generation at 450 nm is typical of phosphorus-related hole centre defects (POHC), which have, with $A \sim 0.7$ cm^{-1}, nearly the same saturation value like FP samples without tin, with $A_{450\,nm} \sim 1.0$ cm^{-1}, but these have at 193 nm a large positive saturation value, $A_{193\,nm} \sim 3.2$ cm^{-1}, attributed to phosphorus-related electron centre defects [4, 15]. It is interesting that the saturation values for the POHC defect generation is reached very fast, after 100–1000 laser pulses also in tin-doped phosphate glasses (Fig. 11, POHC maximum at ~500 nm), but the tin related defect generation goes on. This means that the mechanism has to change from participation of intrinsic to mainly tin-related defect generation. which absorbs in the deep UV region. Fluoride glasses, FP, are more stable regarding intrinsic defect generation by UV lamp irradiation than phosphate and silicate glasses but with 193 nm laser radiation intrinsic defect generation is also possible. Phosphate glasses generate strong intrinsic POHC defects, $\lambda_{max} \sim 500$ nm, with both UV lamp and

laser irradiation (Figs. 9 and 11). The saturation values, $A_{500\,nm}$, without and with tin doping are nearly the same, for HOK lamp, are ~0.3 cm^{-1}, for 248-nm laser ~0.7 cm^{-1}, and for 193-nm laser ~4.5 cm^{-1}. The saturation values in the deep UV region, $A_{\sim200\,nm}$, are totally different, due to tin doping. The induced spectra recorded show superimpositions; further investigations to recognise the mechanism are necessary. P and BS glass samples with nearly the same initial Sn^{2+} content, ~30 ppm, irradiated with UV lamps and lasers, are characterised by a very fast and strong change of the Sn^{2+} s $\rightarrow$ p transitions (Figs. 9–13). The Sn^{2+} absorption bands vanish (negative bands) due to photo-oxidation of Sn^{2+} species and intrinsic EC and HC defects absorbing at $\lambda > 230$ nm are generated. This process depends on the energy density of the UV lamp or laser radiation and can also decreases again after passing a maximum (Figs. 12c and 13). A special Sn-related defect signal was found in the EPR spectra of UV irradiated glass samples, increased with increasing Sn doping. This signal was only very low in X-ray irradiated samples [20].

Sn^{4+} species, which absorb in the shorter UV range (Fig. 2b) should also participate in the defect generation process. A model of defect generation in silicate glasses, doped with As, Sb, Sn, Pb or Ti, very similar to the mechanism of defect generation in FP glasses doped with Pb, is suggested [6, 15, 20]. It can be explained by a two-step absorption process. This includes absorption of UV photons, an energy transfer process between the excited species, introduced by the dopants, and the precursors. The existence of Sn^{2+} or other ions, e.g., As^{3+}, Sb^{3+}, Pb^{2+}, with s^2 electronic configurations, which also show luminescence transitions, is very important for the defect generation. The disappearance of the s^2 ions, which can be detected by the radiation-induced decrease in luminescence, explains the loss of induced extinction after passing through a maximum. In the case of tin-doped glasses, where the redox ratio Sn^{2+}/Sn^{4+} can vary in a wide range between Sn^{2+} and Sn^{4+}, both species can be involved in radiation-induced processes in all three glass types investigated.

5. Conclusions

The intrinsic VUV edge of glasses with low optical basicity is shifted towards longer wavelength in the range FP $\rightarrow$ P $\sim$ BS (Duran with ultra high purity). Charge transfer transitions of Fe^{3+} complexes are dependent on the glass matrix, i.e. the local glass structure. The maximum of the dominating Fe^{3+} band has the lowest intensity and energy in the FP glass with the lowest optical basicity and the most ionic bonding. In the P glass, the energy and intensity are a little higher. The highest energy and intensity were found in the BS glass. The charge-transfer bands for the Fe^{2+} complexes have much lower specific absorption coefficients than those for Fe^{3+} complexes in all glasses investigated.

The three s $\rightarrow$ p transitions for Sn^{2+} are much more influenced by the host glass than the charge-transfer transitions for Fe^{3+} and Fe^{2+} complexes. Their positions are strongly shifted to higher energies (shorter wavelength) in the range BS $\rightarrow$ P $\rightarrow$ FP. The redox ratio is shifted in the same range to the Sn^{2+} state. Sn^{4+} absorption bands (d $\rightarrow$ s) were found at shorter wavelength, near the intrinsic band edge, in all glasses investigated.

UV-lamp- and laser-radiation-induced defects were studied. Photo-oxidation of Fe^{2+} to $(Fe^{2+})^+$–HC and EC-defects depending on the glass matrix with a single-photon mechanism was detected in all glasses. Fe^{3+} species participate in the radiation-induced processes only in silicate glasses. In FP and P glasses they are not able to trap an electron and stabilise a $(Fe^{3+})^-$ defect electron centre.

Sn^{2+} species in FP glasses are very stable against UV lamp, but not against 193-nm laser irradiation. In P and BS glasses, Sn^{2+} species are photo-oxidised also under UV radiation very fast. A two-step mechanism for the defect generation should be assumed. This includes absorption of UV photons, an energy transfer process between the excited Sn^{2+} species and the intrinsic precursors of the glass matrix and visa versa. Defects can change into each other very fast. Both, Sn^{2+} and Sn^{4+} are involved in the radiation-induced processes.

References

[1] T. Westerhoff, K. Knapp, E. Moersen, SPIE 3424 (1998) 10.

[2] D. Ehrt, W. Seeber, J. Non-Cryst. Sol. 129 (1991) 19.

[3] D. Ehrt, M. Carl, T. Kittel, M. Müller, W. Seeber, J. Non-Cryst. Solids 177 (1994) 405.

[4] D. Ehrt, U. Natura, P. Ebeling, J. Non-Cryst. Solids 263–264 (2000) 240.

[5] D. Ehrt, Proc. 2nd Int. Conf. on Borate Glasses, Crystals and Melts, Sofia 1999, Glass Tech. 41 (2000) 182.

[6] U. Natura, D. Ehrt, K. Naumann, Glastech. Ber. Glass Sci. Technol. 74 (2001) 1.

[7] K. Schneider, T. Kloss, Glastech. Ber. Glass Sci. Technol. 68 C2 (1995) 14.

[8] H. Rawson, Inorganic Glass-forming Systems, Academic Press, London, 1967, pp. 108.

[9] D. Möncke, U. Natura, D. Ehrt, Proc. 5th ESG Conference, Prague, Czech Republic, 1999 B4–49.

[10] J.A. Duffy, Phys. Chem. Glasses 38 (1997) 289.

[11] W. Seeber, D. Ehrt, Glastech. Ber. Glass Sci. Technol. 70 (1997) 312.

[12] D. Ehrt, J. Non-Cryst. Sol. 196 (1996) 304.

[13] G.H. Sigel, R.J. Ginther, Glass Technol. 9 (1968) 66.

[14] D. Ehrt, U. Natura, P. Ebeling, M. Müller, Proc. XVIII ICG C10 (1998) 1.

[15] U. Natura, T. Feurer, D. Ehrt, Nucl. Inst. Meth. Phys. Res. B 166–167 (2000) 470.

[16] U. Natura, D. Ehrt, Glastech. Ber. Glass Sci. Technol. 72 (1999) 295.

[17] V.I. Arbuzov, Glass Phys. Chem. 22 (1996) 107.

[18] M. Nofz, Glastech. Ber. Glass Sci. Technol. 72 (1999) 76.

[19] H. Ebendorff-Heidepriem, D. Ehrt, Opt. Mater. 15 (2000) 7.

[20] D. Ehrt, P. Ebeling, U. Natura, U. Kolberg, K. Naumann, S. Ritter, Proc. Int. Congr. Glass, Vol. 1, Invited Papers, Edinburgh, Scotland, 1–6 July, 2001, pp. 84.

[21] D. Ehrt, M. Leister, A. Matthai, Phys. Chem. Glasses 42 (2001) 231.

[22] G. Blasse, B.C. Grabmaier, Luminescent Materials, Springer-Verlag, Berlin, 1994.